Key Points:
- Deforestation influences surface temperature also in locations that are not deforested
- Globally averaged, this temperature change may be stronger than the temperature change at deforested locations
- The surface cooling from changing surface albedo may mainly be nonlocal and thus underestimated in observation-based estimates

Nonlocal Effects Dominate the Global Mean Surface Temperature Response to the Biogeophysical Effects of Deforestation

Johannes Winckler[1,2,3] , **Quentin Lejeune[4,5]** , **Christian H. Reick[1]**, and **Julia Pongratz[1,6]**

[1]Max Planck Institute for Meteorology, Hamburg, Germany, [2]International Max Planck Research School on Earth System Modeling, Hamburg, Germany, [3] Now at Laboratoire des Sciences du Climat et de l'Enviro nnement, Gif-sur-Yvette, France, [4]Institute for Atmospheric and Climate Science, ETH-Zürich, Zurich, Switzerland, [5]Now at Climate Analytics, Berlin, Germany , [6]Ludwig-Maximilians-Universität München, Munich, Germany

Abstract Deforestation influences surface temperature locally ("local effects"), but also at neighboring or remote regions ("nonlocal effects"). Observations indicate that local effects induce a warming in most locations, while many climate models show a global mean cooling when simulating global deforestation. We show that a nonlocal cooling in models, which is excluded from observations, may strongly contribute to these conflicting results. For the MPI-ESM, the globally averaged nonlocal cooling exceeds the globally averaged local warming by a factor of three, for global deforestation but also for realistic areal extents and spatial distributions of deforestation. Furthermore, the globally averaged nonlocal effects dominate the local effects in realistic scenarios across a range of climate models. We conclude that observations alone are not sufficient to capture the full biogeophysical effects, and climate models are needed to better understand and quantify the full effects of deforestation before they are considered in strategies for climate mitigation.

Plain Language Summary Deforestation influences surface temperature at the location of deforestation (local effects) and elsewhere (nonlocal effects). Only the local effects are included in observation-based data sets, but in reality surface temperature may in addition be substantially influenced by the nonlocal effects. Using simulations in a climate model, we show that deforestation-induced changes in the brightness of the surface influence surface temperature mainly nonlocally and thus may be largely overlooked in observation-based data sets. The simulations show that the nonlocal effects have a larger impact on global average surface temperature than the local effects, independent of how much area is deforested and at which latitude the deforestation takes place. A better understanding of the nonlocal effects is essential before the full climate effects of deforestation can be included into international climate policies that aim at mitigating global climate warming.

1. Introduction

Deforestation influences the exchange of heat, moisture, and momentum between the land surface and the atmosphere (Bonan, 2008). These biogeophysical effects impact surface temperature at the location of deforestation ("local effects") which became apparent both in climate modeling studies (Kumar et al., 2013; Lejeune et al., 2017; Malyshev et al., 2015) and global-scale data sets based on observations (Alkama & Cescatti, 2016; Bright et al., 2017; Duveiller et al., 2018; Li et al., 2015). Satellite-based observations measured the difference in surface temperature of forested versus open land either in space (Duveiller et al., 2018; Li et al., 2015) or in time (Alkama & Cescatti, 2016), and a semiempirical approach employed in situ observations from the FLUXNET database (Bright et al., 2017). The observation-based data sets provide valuable information not only for local mitigation and adaptation measures (Bright et al., 2017; Duveiller et al., 2018) but can also serve as a benchmark for the evaluation of local deforestation effects in climate models. Although the underlying methods differ substantially (section 2), these observation-based data sets largely agree that local effects of deforestation induce a warming in most regions, especially in the low and middle latitudes, while there is less agreement about a slight cooling from the local effects of high-latitude deforestation (Figure S1).

Similar to the observations, the biogeophysical effects of global-scale deforestation in climate models induce a warming in low latitudes and a cooling in high latitudes (Davin & de Noblet-Ducoudre, 2010; Devaraju et al., 2015). However, the latitude at which deforestation starts to have a cooling effect is shifted much further south in fully coupled climate models (Zhang et al., 2014). There seems to be a surprising discrepancy between a strong global mean cooling of more than 1.3 K for global deforestation in fully coupled climate models (Bala et al., 2007; Brovkin et al., 2009; Davin & de Noblet-Ducoudre, 2010; Devaraju et al., 2015) and a domination of deforestation-induced warming in the observations.

We hypothesize that this apparent discrepancy is caused by nonlocal cooling effects of deforestation. Climate model simulations showed that large-scale changes in forest cover can result in changes in global-scale circulation patterns (Devaraju et al., 2015; Lague & Swann, 2016; Swann et al., 2012). Such nonlocal effects may also occur through advection and may be amplified through atmospheric and oceanic feedbacks (Davin & de Noblet-Ducoudre, 2010; Gibbard et al., 2005) and can therefore lead to a cooling in areas that were not deforested. On the other hand, in observation-based studies on the effects of deforestation on temperature these nonlocal effects cancel out by construction. Studies based on satellite observations have indeed reported that their methodologies exclude what they called the "atmospheric and oceanic feedbacks" (Li et al., 2015), "second-order effects" (Alkama & Cescatti, 2016), or "large-scale teleconnections" (Duveiller et al., 2018). This is because in these studies the local effects of deforestation are extracted by comparing changes in climate variables over neighboring forested and deforested areas. Therefore, any nonlocal effect triggered by deforestation elsewhere disappears when temperature differences over these neighboring areas are compared. Although it is based on in situ measurements, the same is true for the data set of Bright et al. (2017), whose authors recognize that the "large-scale climate feedbacks" are excluded. Because these four observation-based data sets by construction exclusively contain effects that are locally triggered, they are conceptually comparable to the isolated local effects in the climate models (Kumar et al., 2013; Malyshev et al., 2015). The additional existence of nonlocal deforestation effects in model-based studies is thus a suitable candidate to explain the apparent discrepancy of "mostly warming" in observations and "mostly cooling" in fully coupled climate models.

Here we investigate to what extent a cooling associated with nonlocal effects can explain differences between simulations and observations. In simulations of deforestation with the fully coupled climate model MPI-ESM (Giorgetta et al., 2013) we use a recently developed method (Winckler et al., 2017a) to separate local and nonlocal biogeophysical effects, and then compare the local effects to the observations. Using this framework, we also address some aspects of the nonlocal effects which are still poorly understood. For instance, it is unclear whether the nonlocal effects only affect global mean surface temperature in scenarios of large-scale deforestation or also in more realistic deforestation scenarios. These two types of studies differ in the areal extent and in the spatial distribution of deforestation, both of which may influence the nonlocal effects (Devaraju et al., 2015; Lawrence & Vandecar, 2014). To bridge this gap between simulations of large-scale deforestation and more realistic deforestation scenarios we investigate idealized deforestation scenarios: We analyze the local and nonlocal effects of different areal extents of deforestation, and we study how the nonlocal effects depend on the spatial distribution of deforestation by analyzing the nonlocal effects on global mean surface temperature in simulations of deforestation in three latitudinal bands. Furthermore, we assess the role of changes in surface albedo by analyzing a simulation in which only the surface albedo is changed from forest to grass values. Finally, using realistic deforestation scenarios (historical deforestation 1860–2000, Pongratz et al., 2010, and possible future deforestation 2006–2100, Brovkin, Boysen, Arora, et al., 2013), we assess the robustness of the nonlocal effects by comparing changes in global mean surface temperature across a wide range of climate models.

2. Methods

2.1. Model Description of the MPI-ESM

The climate model MPI-ESM (Giorgetta et al., 2013) consists of the atmospheric model ECHAM6 (Stevens et al., 2013) that is coupled to the ocean model MPIOM (Jungclaus et al., 2013) and the land surface model JSBACH (Reick et al., 2013). Surface albedo is calculated interactively and depends on the background soil albedo, soil moisture, snow cover, and vegetation cover. The MPI-ESM has been evaluated with respect to key land surface variables (Brovkin, Boysen, Raddatz, et al., 2013; Hagemann et al., 2013). In particular, surface albedo agrees reasonably well with observations (Brovkin, Boysen, Raddatz, et al., 2013) and responds to deforestation by an albedo increase (snow-free surface albedo increases approximately from 0.13 to 0.19 at

a location of 100% deforestation, not shown), that is, at the lower end but within the range of other climate models (Boisier et al., 2013; Lejeune et al., 2017). Soil moisture is calculated interactively in a five-layer soil hydrology model (Hagemann et al., 2013). Soil water is shared between plant functional types within a grid cell, and there is no horizontal exchange of soil water between neighboring grid cells. Surface temperature in the MPI-ESM is calculated by solving the surface energy balance equation in a bulk canopy layer. The surface temperature in the MPI-ESM can consistently be compared to screen temperature based on observations of terrestrial radiation (Winckler et al., 2018). A similar quantity to the local effects that we isolate here could also be obtained by comparing surface temperature between "tiles" covered by different subgrid vegetation types within a grid cell (Malyshev et al., 2015; Meier et al., 2018; Schultz et al., 2016) or by simulations using an offline land surface model (Gibbard et al., 2005). However, these approaches cannot account for changes in the atmosphere (cloud cover, precipitation, etc.) that would be triggered locally by deforestation, such that part of the local temperature change induced by the interaction with the atmosphere is missing in the identification of the local signal. Details on the calculation of surface temperature in the MPI-ESM and the different response of surface and air temperature to deforestation are also provided in Winckler et al. (2018).

2.2. Simulations Performed With the MPI-ESM

We use the MPI-ESM to perform simulations of deforestation. For all simulations, we use an interactive ocean because this was shown to be essential for capturing the full biogeophysical response to changes in forest cover (Davin & de Noblet-Ducoudre, 2010). We run each simulation experiment with a horizontal atmospheric resolution of 1.9° for 350 years and analyze the last 200 years. In order to only simulate the biogeophysical effects, we prescribe CO_2 concentrations at preindustrial level.

An overview of all simulations is provided in Table S1. We simulate climate in a forest world where forest cover is prescribed in the vegetated part of all model grid cells, that is, to the extent that vegetation can grow within a grid cell (Reick et al., 2013; see Figure S2), such that forest is not prescribed in desert areas. The vegetated part in each grid cell is taken from a previous study (Pongratz et al., 2008) where it was reconstructed from satellite-based potential vegetation (Ramankutty & Foley, 1999). We also prescribe forest in, for example, present-day grasslands in arid areas because many of these areas can potentially be afforested, and an afforestation there can also substantially influence climate (Rotenberg & Yakir, 2010).

In order to investigate the sensitivity of the nonlocal effects to an increasing deforestation area, we completely replace forest by grasslands in one out of four, two out of four, or three out of four grid cells (simulations "1/4," "2/4," and "3/4"). These grid cells are distributed in a regularly spaced pattern (colored in Figures S3a–S3c).

A better understanding of the nonlocal effects requires knowledge about the location of forest cover change from where the nonlocal effects are triggered. While a given realization of nonlocal effects cannot be attributed to a specific location of forest cover change, we can constrain the nonlocal effects to forest cover change of the high, intermediate, and low latitudes by simulating deforestation in these latitudinal bands separately (simulations "low lats" [17°S–17°N], "intermediate lats" [17°–41°S and 17°–41°N], and "high lats" [>41°S and >41°N]). The exact latitudes were chosen such that the areal extents of forest cover change (about twice the historically deforested area) are approximately equal to the areal extent in the 1/4 simulation in all three simulations, so that their comparison identifies the relevance of the spatial distribution of forest cover change. To also capture the nonlocal effects of a more realistic spatial distribution, we change forest cover in the same areal extent but we locate the forest cover change grid cells near areas that were historically deforested (simulation "2x_historical"). To determine which grid cells are chosen as deforestation grid cells in 2x_historical, we rank all land grid cells according to the fraction of the grid cells that was deforested in the "historical" simulation in CMIP5. We then choose the grid cells with the highest deforestation fraction until their cumulative areal extent is equal to the areal extent in the scenario 1/4. In these four simulations, we change forest cover in only three of four grid cells in the respective region, so we are still able to separate local and nonlocal effects.

While in these simulations all surface properties (albedo, evapotranspiration efficiency, surface roughness) are changed between forest to grass values, in an additional simulation we only change surface albedo in three out of every four grid cells (simulation "only albedo"). This allows us to assess the role of changes in surface albedo for the local and nonlocal effects separately.

2.3. Separation of Local and Nonlocal Effects in the MPI-ESM

In the simulations described above, we separate local and nonlocal effects as follows (Winckler et al., 2017a): We simulate forest cover change in some grid cells while keeping the forest in other grid cells. We define the "nonlocal effects" as the signal that is also apparent in grid cells where forest cover in our simulations is not changed. The nonlocal effects are spatially interpolated to the grid cells located in between where forest cover is changed. At these grid cells we then define the local effects as the simulated signal minus the nonlocal effects. For comparability of the local effects in the MPI-ESM (Figure 1) with the observation-based data sets (Figure S1), the local effects are spatially interpolated also to the grid cells where forest cover is not changed. This approach of isolating the local effects (Winckler et al., 2017a) is similar to the space-for-time–substitution performed in the study by Li et al. (2015) to isolate the local effects of "potential deforestation" (Li et al., 2016) from remote-sensing observations. The key difference between their and our approach is that they define the local effects as the difference in "temperature" between nearby locations with and without forests, while we consider differences in the "response of temperature to deforestation" between nearby locations with and without deforestation.

2.4. Isolation of Local and Nonlocal Effects Across Models

In order to compare local and nonlocal effects across climate models, we isolate the local effects from existing simulations of the biogeophysical effects of deforestation in other fully coupled climate models. For this particular set of existing simulations (historical, RCP2.6 and RCP8.5, see Table S2), we cannot use the separation approach described above because deforestation in these realistic scenarios does not happen in a regular spatial pattern that includes no-deforestation grid cells. Thus, we isolate the local effects by using the moving-window approach of Lejeune et al. (2018), which is explained and compared to an alternative approach (Winckler et al., 2017b) in Text S1.

2.5. Comparison of Simulation Results to Observational Data Sets

We compare simulated local effects on surface temperature in the MPI-ESM to three data sets inferred from satellite observations (Alkama & Cescatti, 2016; Duveiller et al., 2018; Li et al., 2015) and one semiempirical data set (Bright et al., 2017) based on FLUXNET observations. As described in section 1, this comparison is only methodologically consistent for the model's local effects because the observations only contain local effects. Although the observations depict real-world forest cover changes while the scenarios used in our simulations are idealized ones, the model-data comparison (here: to the simulation 3/4) is valid for two reasons: First, the observations contrast surface temperature at a location with 100% forest to the same or nearby location with 0% forest ("potential" instead of "actual" deforestation; Li et al., 2016), which is comparable to what we have in our simulation setup. Second, the simulated local effects at one location are largely independent of deforestation elsewhere (Winckler et al., 2017a), and thus the local effects are not substantially influenced by the nonlocal effects in this large-scale deforestation scenario. Text S2 provides details on the observation-based data sets (in which respects they differ and how they are latitudinally averaged for Figure 1).

2.6. Two Perspectives on the Comparison of Local and Nonlocal Effects

In section 3, we compare local and nonlocal biogeophysical deforestation effects on simulated changes in surface temperature in two different ways:

The *grid-cell perspective* focuses on the average local/nonlocal temperature change over selected deforested grid cells (in our simulations, the grid cells do not necessarily have to be deforested—the local/nonlocal temperature change for a hypothetical deforestation can also be derived from interpolation). The average can be calculated for deforested grid cells in a region, in latitudinal bands, or all deforested grid cells globally. By contrast, the *global perspective* focuses on the average over all grid cells worldwide independently of whether these grid cells are deforested or not. This global perspective would be taken, for example, for land use in the context of climate change mitigation.

Formally the situation is the following. The temperature change ΔT_n in a grid cell n can be separated into local and nonlocal contributions:

$$\Delta T_n = (\Delta T_n)_{local} + (\Delta T_n)_{nonlocal} \tag{1}$$

According to the grid-cell perspective, the average temperature change over these grid cells (weighted by the grid cell area) can be calculated as follows (here for the local contribution):

$$\langle \Delta T_n \rangle_{local}^{(gc)} = \frac{\sum_{n=1}^{N_{defor}} (\Delta T_n)_{local} \cdot A_n}{\sum_{n=1}^{N_{defor}} A_n}, \tag{2}$$

where N_{defor} denotes the number of considered grid cells and A_n denotes the area of a grid cell n. In contrast, according to the global perspective, the contribution of the local temperature change to global average temperature change can be calculated as follows:

$$\langle \Delta T_n \rangle_{local}^{(ww)} = \frac{\sum_{n=1}^{N_{global}} (\Delta T_n)_{local} \cdot A_n}{\sum_{n=1}^{N_{global}} A_n} \tag{3}$$

Here the summation concerns all grid cells worldwide. In fact, $(\Delta T_n)_{local}$ is nonzero in equation (3) only at deforested grid cells so that the major difference between the two averages is the division either by the spatial extent only of deforested grid cells in the respective region $\left(\sum_{n=1}^{N_{defor}} A_n \right)$ or all grid cells worldwide $\left(\sum_{n=1}^{N_{global}} A_n \right)$. For the global perspective, this normalization by global area is needed for $\langle \Delta T \rangle_{local}^{(ww)}$ to be interpreted as the contribution from local temperature changes to the global average temperature change $\langle \Delta T \rangle^{(ww)}$, namely,

$$\langle \Delta T \rangle^{(ww)} = \langle \Delta T \rangle_{local}^{(ww)} + \langle \Delta T \rangle_{nonlocal}^{(ww)}, \tag{4}$$

where $\langle \Delta T \rangle_{nonlocal}^{(ww)}$ is calculated analogously to equation (3).

Figure 1 shows the temperature changes averaged over deforested grid cells (equation (2) for local and nonlocal contributions, respectively). Here N_{defor} refers to all grid cells in a given latitude for which at least one observational data set was available. In contrast, Figure 2 shows the contributions to global mean temperature change (equation (3) for local and nonlocal contributions, respectively). The global averages are calculated for simulations with different areal extents of deforestation. The local contributions to global mean temperature change scales with number of deforested grid cells (i.e., number of grid cells with nonzero $(\Delta T_n)_{local}$) and the nonlocal contribution may scale with strength of temperature change in all grid cells (i.e., values of $(\Delta T_n)_{nonlocal}$). The nonlocal contribution to temperature changes in Figure 1 is calculated by equation (2), that is, consistently with the local contribution to temperature changes. However, the strength of temperature change from nonlocal effects in each grid cell depends of course on the extent of deforestation; in Figure 1 we use the 3/4 scenario, as discussed in the second paragraph of the results.

3. Results

3.1. Local Effects in the MPI-ESM and Observations

We find that, at most latitudes, the local effects of deforestation in the MPI-ESM lead to changes in surface temperature that lie at the lower end of the satellite-based data sets (Alkama & Cescatti, 2016; Duveiller et al., 2018; Li et al., 2015; Figures 1 and S1), and the local effects in the MPI-ESM largely agree with the in situ-based data set (Bright et al., 2017). This overall agreement indicates that the employed model captures the most essential processes by which deforestation influences surface temperature locally, even if the full complexity of plant processes is represented in the model by a simplified vegetation parametrization. There are a few regions where the simulated local effects agree less well with those in the observations, for example, in the southern-hemisphere tropics. This may be either due to a misrepresentation of some processes in MPI-ESM or due to observational biases because of high cloud cover in the satellite-based observations (Alkama & Cescatti, 2016; Duveiller et al., 2018; Li et al., 2015) and the sparse spatial coverage of flux tower measurements there (Bright et al., 2017).

Nonlocal effects are not included in the observation-based data sets, so they prevent a consistent comparison between the total deforestation effects simulated by climate models and those captured by observations. While the local effects within a grid cell are largely independent of deforestation elsewhere (Winckler et al., 2017a), the nonlocal effects on surface temperature may strongly depend on the location and spatial extent of deforestation, which we will investigate in the following paragraphs. In order to assess how strongly the nonlocal effects can contribute to an apparent mismatch between models and observations, we compare the
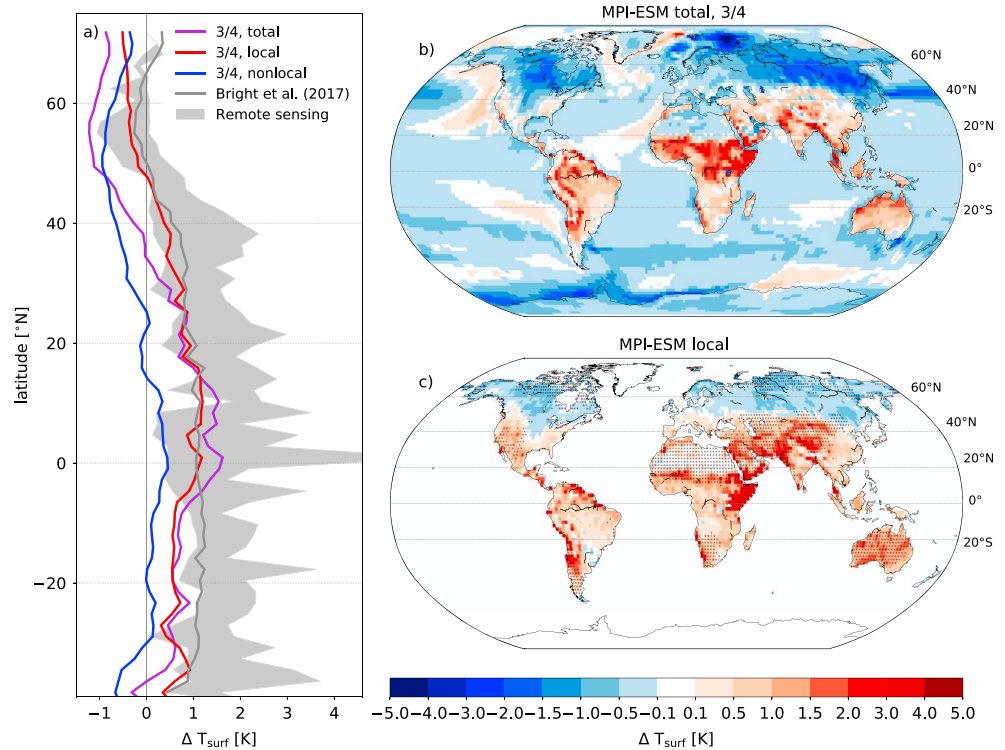
Figure 1. Comparison of biogeophysical effects of deforestation on surface temperature in the MPI-ESM versus observations. The shaded area in (a) indicates the range of three remote-sensing-based data sets (Alkama & Cescatti, 2016; Duveiller et al., 2018; Li et al., 2015) and the gray line indicates an in situ-based data set (Bright et al., 2017). The colored lines indicate total, local, and nonlocal effects when simulating the deforestation in three of four grid cells ("3/4") in the coupled climate model MPI-ESM. For the latitudinal averages in (a), values in the MPI-ESM are averaged (as calculated from equation (2)) over areas where values in at least one of the observational data sets is available (land grid cells in (c) that are not stippled). The results for the MPI-ESM are shown in (b) for the total (local plus nonlocal) and (c) local effects, here extrapolated to all land grid cells. The map of the nonlocal effects is shown in Figure S3h, and maps of the observation-based data sets are shown in Figure S1.

observations to the changes in surface temperature of deforestation in three out of four grid cells (simulation 3/4, see section 2). In this scenario, a large area is deforested but we can still separate local and nonlocal effects. We find that in this scenario the nonlocal effects contribute to a cooling of up to −0.9 K in the regions of the northern middle and high latitudes where observations are available and the nonlocal cooling is strong enough to push the total effects outside of the observational range (Figure 1).

3.2. Investigating the Nonlocal Effects in the MPI-ESM for Idealized Scenarios

The areal extent of deforestation affects global mean surface temperature both for the local and nonlocal effects. Spatially homogeneous deforestation of three of four grid cells in the MPI-ESM results in a global mean biogeophysical surface cooling of approximately −0.2 K, and this total cooling consists of a warming of approximately 0.1 K for the local effects and a cooling of approximately −0.3 K for the nonlocal effects. Maps for the annual and seasonal values are shown in Figures S3 and S4. The simulated ratio of 1:−3 between global mean local warming and nonlocal cooling remains constant in simulations where deforestation is imposed using a similar spatially homogeneous pattern but with a smaller areal extent of deforestation (deforestation in only one or two of four grid cells, i.e., simulations 1/4 and 2/4). Thus, in contrast to previous studies (Lawrence & Vandecar, 2014), we find that both local and nonlocal contributions to global mean temperature change scale linearly with the number of deforested grid cells (see also maps in Figure S3). This suggests that the nonlocal effects may dominate the globally averaged response not only when simulating idealized large-scale deforestation, but also when simulating smaller areal extents, such as historical deforestation (Pongratz et al., 2009) or the even smaller extent of deforestation that is projected for the next century (Brovkin, Boysen, Arora, et al., 2013).
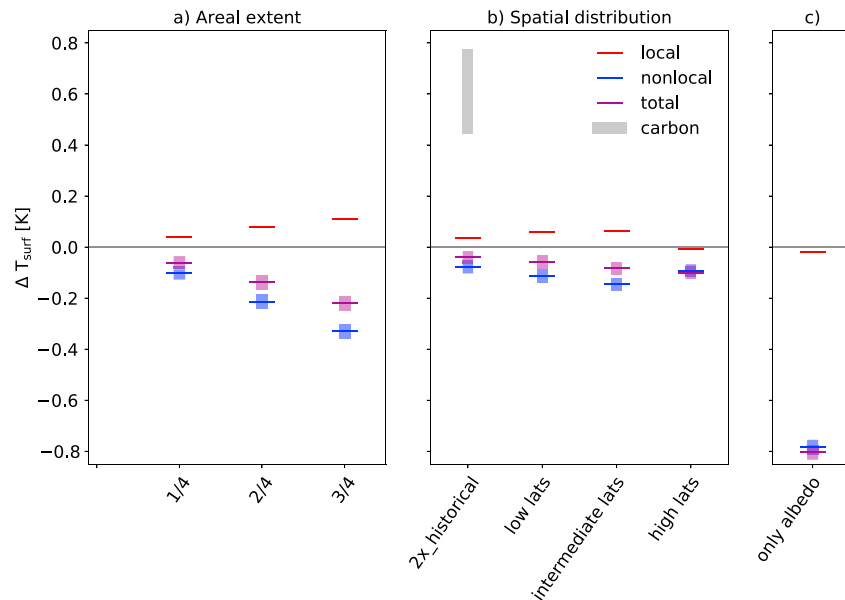
AGU
100
ADVANCING EARTH
AND SPACE SCIENCE

Geophysical Research Letters

10.1029/2018GL080211

Figure 2. Separation of the global mean surface temperature response from the total biogeophysical effects of deforestation into contributions from local and nonlocal effects. (a) Temperature response to varying the areal extent of deforestation (one, two, or three out of every four grid cells globally). (b) Temperature response to varying the location of deforestation (near historically deforested areas or in low, intermediate, and high latitudes). (c) Temperature response in a simulation where only surface albedo is changed (section 2). To set the biogeophysical effects into context, we provide an estimate of the temperature increase due to land carbon loss associated with the "2x_historical" scenario (gray bar in *b*, "carbon"); the corresponding values are obtained using a bookkeeping approach (Hansis et al., 2015) and the transient response to cumulative emissions (Gillett et al., 2013; for details see Text S3). The thin horizontal lines denote global mean values and the colored rectangles denote the 95% confidence intervals of the means. For the local effects, the confidence intervals are so narrow that the corresponding rectangles are not visible. The global mean changes in surface temperature (calculated from equation (3)) are statistically significant ($\alpha = 5\%$, Zwiers & von Storch, 1995) for all simulations. Maps showing the statistical significance for the total (local plus nonlocal) effects are shown in Figure S9.

Not only the areal extent, but also the spatial distribution of deforestation influences the resulting climate effects. While the 1:−3 ratio was obtained by simulations in which deforestation is distributed homogeneously across the globe, the nonlocal cooling also dominates in simulations in which the areal extent is equal to the extent in the simulation 1/4 but in which deforestation is restricted to specific locations. In the simulation with a more realistic spatial distribution of deforestation (2x_historical), in which deforestation is simulated following a spatial pattern similar to that of historical deforestation but over twice its areal extent (colored grid cells in Figure S3d and section 2), the surface cooling from the nonlocal effects is more than twice the warming from the local effects. Furthermore, the nonlocal effects exert a global mean cooling for deforestation in all three latitudinal bands (Figure 2b). For high-latitude deforestation, this cooling is in line with the total biogeophysical effects found in previous studies (Betts, 2000; Bonan et al., 1992; Mahmood et al., 2014). Surprisingly, the nonlocal cooling is even stronger in our simulations of deforestation of the low and intermediate latitudes (Figures 2b and S5).

The global mean nonlocal cooling signal of low-latitude deforestation challenges the wide-spread idea that tropical deforestation induces a warming (Bonan, 2008; Mahmood et al., 2014). Three aspects shed light into this apparent contradiction: First, while we consider only biogeophysical effects, some studies included the effects of land carbon losses related to tropical deforestation (Bala et al., 2007; Bathiany et al., 2010), which lead to a strong warming. Second, some studies only consider the local effects (Alkama & Cescatti, 2016; Bright et al., 2017; Duveiller et al., 2018; Li et al., 2015) or at least include the local effects (Claussen et al., 2001), and we also find in our simulations that the global mean local effects of low-latitude deforestation are warming (Figure 2b). Third, even in our simulations the nonlocal effects cause a regional surface warming of the low latitudes (Figure S5) because of a regional decrease in shortwave incoming radiation (Figure S6). However, low-latitude deforestation decreases atmospheric water vapor (Claussen et al., 2001) and thus at

the same time triggers a nonlocal cooling that extends much beyond the deforested regions (Figure S5) and dominates the global average (Figure 2b).

Changes in surface albedo have been identified as the driver of the biogeophysical cooling in deforestation simulations (Davin & de Noblet-Ducoudre, 2010). For a better understanding of the cooling, we separate local and nonlocal effects resulting from a change in only surface albedo from forest to grass values while preserving all other surface properties. As expected, an increase in surface albedo leads to a cooling in both the local and nonlocal effects because more solar incoming radiation is reflected by the brighter surface. Our simulations show that the vast majority of this cooling is excluded from the local effects (Figures 2c and S3) because within brightened or deforested grid cells the decrease in net solar radiation is largely balanced by a reduction of latent and sensible heat fluxes (Figure S7). The albedo-induced cooling is weak in the local effects, and the observations only show the local effects. Thus, the albedo-induced cooling may be lacking in the observations.

The albedo-induced cooling is mainly a nonlocal effect (Figures 2c and S3). Following the argumentation from a previous study (Davin & de Noblet-Ducoudre, 2010), we hypothesize that advection plays a key role in the albedo-induced nonlocal cooling. Within a brightened or deforested location, the reduced input of sensible and latent heat (Figure S7) cools and dries the air. This cooler and drier air may be mixed into higher atmospheric levels and carried to neighboring and remote grid cells via advection. Consistent with the earlier study (Davin & de Noblet-Ducoudre, 2010), longwave incoming radiation is reduced (Figure S6) also at land locations that were not deforested and over the oceans. In addition, changes in cloud cover (not shown) can lead to changes in shortwave incoming radiation. Both changes in shortwave and longwave incoming radiation require the interactive simulation of atmospheric processes and would not be seen in simulations using a stand-alone land model (Gibbard et al., 2005). The spatial pattern of nonlocal changes in total (shortwave plus longwave) incoming radiation closely resembles the spatial pattern of nonlocal changes in surface temperature (Figure S6). This suggests that, while the local temperature response to deforestation is driven by nonradiative processes (Bright et al., 2017), the radiative processes are essential for the nonlocal (and thus also the full) temperature response.

3.3. Intermodel Comparison of Nonlocal Effects for Historical and Future Deforestation Scenarios

We investigate whether the nonlocal cooling is only apparent in the MPI-ESM or also in other climate models. The global mean cooling in the MPI-ESM is rather small in comparison to other models that simulate a biogeophysical cooling between -1.3 K and -1.6 K in response to global-scale deforestation (Bala et al., 2007; Davin & de Noblet-Ducoudre, 2010; Devaraju et al., 2015). While in the previous paragraphs we investigated the climate effects of idealized large-scale changes in forest cover, we now focus on more realistic scenarios of deforestation and assess the robustness of the nonlocal cooling across a wide range of fully coupled climate models (Figure 3). We isolate the local biogeophysical effects in existing simulations (Lejeune et al., 2018, see also Text S1) of historical deforestation (between 1860 and 2005; Pongratz et al., 2009) and future deforestation (scenarios RCP2.6 and RCP8.5 between 2006 and 2100; Brovkin, Boysen, Arora, et al., 2013; Moss et al., 2010), and we define the nonlocal effects as the simulated total minus local effects.

Consistently with our idealized experiments in the MPI-ESM, the nonlocal effects induce a cooling for five of the six models in the case of historical deforestation, although there is a substantial spread of the ensemble members within the individual models. The picture is less clear in the RCP2.6 and RCP8.5 scenarios of future deforestation. This could be due to the lower number of ensemble members compared to historical deforestation (see Table S2). Within one model, the spread across the ensemble members is much smaller for the local effects (most values in Figure 3 are plotted on top of each other) than for the nonlocal effects because the climate variability is by construction largely included in the nonlocal effects (Kumar et al., 2013; Lejeune et al., 2017). The method that we use here to isolate the local effects might underestimate the local effects (Lejeune et al., 2018, and Figure S8).

One possible explanation for the spread between individual models in Figure 3 is the differences in vegetation parametrization. For example, the GFDL-ESM2 has separate soil moisture reservoirs for grasses and trees, which is important for capturing the changes in transpiration due to anthropogenic land use and land cover change (Findell et al., 2017). A reduced evapotranspiration could potentially translate into a warming also elsewhere, for example, via a reduction of low-level clouds (Ban-Weiss et al., 2011), which may explain the nonlocal warming in the GFDL-ESM2. This hypothesis suggests that the exact magnitude of nonlocal
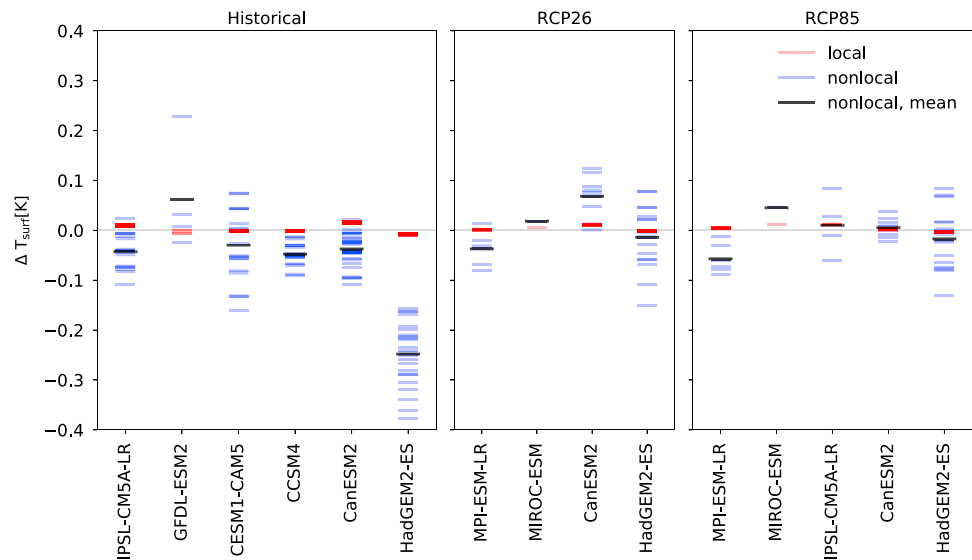
Figure 3. Comparison of local and nonlocal effects across models. Shown are annual mean changes in global mean surface temperature (K) for the local effects (red) and for the nonlocal effects (blue: different combinations of ensemble members, black: mean of all available ensemble members [section 2, Text S1, and Table S2]). Shown are averages over the last 30 years of historical deforestation (years 1860–2000) and deforestation in the RCP2.6 and RCP8.5 scenario (years 2006–2100).

warming or cooling in a model depends on the balance between the albedo increase and the transpiration decrease following deforestation. The relative importance of nonlocal effects differs in quantitative terms across models and the ratio of 1:−3 found for the MPI-ESM is certainly model-specific. However, in all models analyzed here the nonlocal effects seem to be of substantial importance.

Another factor that may substantially influence the deforestation effects in the models lies in the representation of oceanic processes. The inclusion of an interactive ocean can substantially influence the simulated results (Davin & de Noblet-Ducoudre, 2010; Ganopolski et al., 2001). When imposing the SSTs, the nonlocal effects may be reduced, which may also explain why only small remote effects were found in a study simulating large-scale Amazon deforestation (Lorenz et al., 2016). On the other hand, a previous intermodel comparison using prescribed sea surface temperatures ("LUCID"; de Noblet-Ducoudré et al., 2012; Pitman et al., 2009) found a global mean cooling for historical deforestation in six of seven models (de Noblet-Ducoudré et al., 2012; Pitman et al., 2009) which is roughly consistent with the results that we get here using an interactive ocean (Figure 3). Other studies (Devaraju et al., 2015; Gibbard et al., 2005; Jones et al., 2013; Swann et al., 2012) use a slab ocean ("mixed-layer ocean," about 50 m deep) to account for changes in the ocean heat uptake; however, the "transport" of oceanic heat in their simulations is prescribed, and it is unclear whether this influences the nonlocal effects. The current coordinated effort to investigate the biogeophysical effects of land use and land cover change ("LUMIP"; Lawrence et al., 2016) includes simulations with a fully coupled ocean that account for all ocean feedbacks.

4. Conclusions

Forests have been identified as a key component for the mitigation of global climate change (Grassi et al., 2017; Griscom et al., 2017) because they enhance the land carbon sink (Le Quéré et al., 2018). Moreover, recent observation-based studies on the local effects (Alkama & Cescatti, 2016; Bright et al., 2017; Duveiller et al., 2018; Li et al., 2015) suggested that afforestation would bring additional co-benefits through a local biogeophysical cooling. However, when including their nonlocal contribution, we find that the biogeophysical effects may overall reduce the carbon-related climate benefits of afforestation for global mean surface temperature (estimated as "carbon" in Figure 2b, see section 2). The exact values of the nonlocal effects may depend on the vegetation parametrization and thus on the employed climate model, but the fact that the globally averaged nonlocal effects are at least as important as the local effects is robust across the models. Thus, if the biogeophysical effects were to be considered in climate policies to regulate global mean temper-

ature, we stress that their nonlocal components would need to be better understood so that their important contribution is not missed out, and their potentially counterproductive consequences are not overlooked.

We conclude that the local effects alone—and thus also observations—only yield an incomplete picture of the climatic consequences of deforestation. The nonlocal effects can strongly contribute to the mismatch between models and observations because the albedo-induced cooling is largely excluded from the local effects and thus from observation-based data sets. Because the current observations do not include the nonlocal effects, climate models are essential to better understand and quantify the full climate effects of deforestation.

References

Alkama, R., & Cescatti, A. (2016). Biophysical climate impacts of recent changes in global forest cover. *Science*, *351*, 600–604. https://doi.org/10.1126/science.aac8083

Bala, G., Caldeira, K., Wickett, M., Phillips, T. J., Lobell, D. B., Delire, C., & Mirin, A. (2007). Combined climate and carbon-cycle effects of large-scale deforestation. *Proceedings of the National Academy of Sciences*, *104*(16), 6550–6555. https://doi.org/10.1073/pnas.0608998104

Ban-Weiss, G. A., Bala, G., Cao, L., Pongratz, J., & Caldeira, K. (2011). Climate forcing and response to idealized changes in surface latent and sensible heat. *Environmental Research Letters*, *6*, 1–8. https://doi.org/10.1088/1748-9326/6/3/034032

Bathiany, S., Claussen, M., Brovkin, V., Raddatz, T., & Gayler, V. (2010). Combined biogeophysical and biogeochemical effects of large-scale forest cover changes in the MPI Earth system model. *Biogeosciences*, *7*, 1383–1399. https://doi.org/10.5194/bg-7-1383-2010

Betts, R. A. (2000). Offset of the potential carbon sink from boreal forestation by decreases in surface albedo. *Nature*, *408*, 187–190.

Boisier, J. P., de Noblet-Ducoudre, N., & Ciais, P. (2013). Inferring past land use-induced changes in surface albedo from satellite observations: A useful tool to evaluate model simulations. *Biogeosciences*, *10*, 1501–1516. https://doi.org/10.5194/bg-10-1501-2013

Bonan, G. B. (2008). Forests and climate change: Forcings, feedbacks, and the climate benefits of forests. *Science*, *320*, 1444–1449. https://doi.org/10.1126/science.1155121

Bonan, G. B., Pollard, D., & Thompson, S. L. (1992). Effects of boreal forest vegetation on global climate. *Nature*, *359*, 716–718. https://doi.org/Doi 10.1038/359716a0

Bright, R. M., Davin, E. L., O'Halloran, T. L., Pongratz, J., Zhao, K., & Cescatti, A. (2017). Local temperature response to land cover and management change driven by non-radiative processes. *Nature Climate Change*, *7*, 296–302. https://doi.org/10.1038/nclimate3250

Brovkin, V., Boysen, L., Arora, V. K., Boisier, J. P., Cadule, P., Chini, L., et al. (2013). Effect of anthropogenic land-use and land-cover changes on climate and land carbon storage in CMIP5 projections for the twenty-first century. *Journal of Climate*, *26*, 6859–6881. https://doi.org/10.1175/JCLI-D-12-00623.1

Brovkin, V., Boysen, L., Raddatz, T., Gayler, V., Loew, A., & Claussen, M. (2013). Evaluation of vegetation cover and land-surface albedo in MPI-ESM CMIP5 simulations. *Journal of Advances in Modeling Earth Systems*, *5*, 48–57. https://doi.org/10.1029/2012MS000169

Brovkin, V., Raddatz, T., Reick, C. H., Claussen, M., & Gayler, V. (2009). Global biogeophysical interactions between forest and climate. *Geophysical Research Letters*, *36*, L07405. https://doi.org/10.1029/2009GL037543

Claussen, M., Brovkin, V., & Ganopolski, A. (2001). Biogeophysical versus biogeochemical feedbacks of large-scale land cover change. *Geophysical Research Letters*, *28*, 1011–1014.

Davin, E. L., & de Noblet-Ducoudre, N. (2010). Climatic impact of global-scale deforestation: Radiative versus nonradiative processes. *Journal of Climate*, *23*(1), 97–112. https://doi.org/10.1175/2009JCLI3102.1

de Noblet-Ducoudré, N., Boisier, J. P., Pitman, A., Bonan, G. B., Brovkin, V., Cruz, F., et al. (2012). Determining robust impacts of land-use-induced land cover changes on surface climate over North America and Eurasia: Results from the first set of LUCID experiments. *Journal of Climate*, *25*, 3261–3281. https://doi.org/10.1175/JCLI-D-11-00338.1

Devaraju, N., Bala, G., & Modak, A. (2015). Effects of large-scale deforestation on precipitation in the monsoon regions: Remote versus local effects. *Proceedings of the National Academy of Sciences*, *112*, 3257–3262. https://doi.org/10.1073/pnas.1423439112

Duveiller, G., Hooker, J., & Cescatti, A. (2018). A dataset mapping the potential biophysical effects of vegetation cover change. *Scientific Data*, *5*, 1–15. https://doi.org/10.1038/sdata.2018.14

Duveiller, G., Hooker, J., & Cescatti, A. (2018). The mark of vegetation change on Earth's surface energy balance. *Nature Communications*, *9*(1), 1–12. https://doi.org/10.1038/s41467-017-02810-8

Findell, K. L., Berg, A., Gentine, P., Krasting, J. P., Lintner, B. R., Malyshev, S., et al. (2017). The impact of anthropogenic land use and land cover change on regional climate extremes. *Nature Communications*, *8*(1), 1–9. https://doi.org/10.1038/s41467-017-01038-w

Ganopolski, A., Petoukhov, V., Rahmstorf, S., Brovkin, V., Claussen, M., Eliseev, A., & Kubatzki, C. (2001). CLIMBER-2: A climate system model of intermediate complexity. Part II: Model sensitivity. *Climate Dynamics*, *17*, 735–751.

Gibbard, S., Caldeira, K., Bala, G., Phillips, T. J., & Wickett, M. (2005). Climate effects of global land cover change. *Geophysical Research Letters*, *32*, L23705. https://doi.org/10.1029/2005GL024550

Gillett, N. P., Arora, V. K., Matthews, D., & Allen, M. R. (2013). Constraining the ratio of global warming to cumulative CO_2 emissions using CMIP5 simulations. *Journal of Climate*, *26*, 6844–6858. https://doi.org/10.1175/JCLI-D-12-00476.1

Giorgetta, M. A., Roeckner, E., Mauritsen, T., Bader, J., Crueger, T., Esch, M., & Stevens, B. (2013). The atmospheric general circulation model ECHAM6—Model description (*135*). Hamburg: Max-Planck-Institute for Meteorology.

Grassi, G., House, J., Dentener, F., Federici, S., den Elzen, M., & Penman, J. (2017). The key role of forests in meeting climate targets requires science for credible mitigation. *Nature Climate Change*, *7*, 220–228. https://doi.org/10.1038/nclimate3227

Griscom, B. W., Adams, J., Ellis, P. W., Houghton, R. A., Lomax, G., Miteva, D. A., et al. (2017). Natural climate solutions. *Proceedings of the National Academy of Sciences*, *114*(44), 11,645–11,650. https://doi.org/10.1073/pnas.1710465114

Hagemann, S., Loew, A., & Andersson, A. (2013). Combined evaluation of MPI-ESM land surface water and energy fluxes. *Journal of Advances in Modeling Earth Systems*, *5*, 259–286. https://doi.org/10.1029/2012MS000173

Hansis, E., Davis, S. J., & Pongratz, J. (2015). Relevance of methodological choices for accounting of land use change carbon fluxes. *Global Biogeochemical Cycles*, *29*, 1230–1249. https://doi.org/10.1002/2014GB004997

Jones, A. D., Collins, W. D., & Torn, M. S. (2013). On the additivity of radiative forcing between land use change and greenhouse gases. *Geophysical Research Letters*, *40*, 4036–4041. https://doi.org/10.1002/grl.50754

Jungclaus, J. H., Fischer, N., Haak, H., Lohmann, K., Marotzke, J., Matei, D., et al. (2013). Characteristics of the ocean simulations in the Max Planck Institute Ocean Model (MPIOM) the ocean component of the MPI-Earth system model. *Journal of Advances in Modeling Earth Systems*, *5*, 422–446. https://doi.org/10.1002/jame.20023

Kumar, S., Dirmeyer, P. a., Merwade, V., DelSole, T., Adams, J. M., & Niyogi, D. (2013). Land use/cover change impacts in CMIP5 climate simulations: A new methodology and 21st century challenges. *Journal of Geophysical Research: Atmospheres*, *118*, 6337–6353. https://doi.org/10.1002/jgrd.50463

Lague, M., & Swann, A. (2016). Progressive midlatitude afforestation: Impacts on clouds, global energy transport, and precipitation. *Journal of Climate*, *29*, 5561–5573. https://doi.org/10.1175/JCLI-D-15-0748.1

Lawrence, D. M., Hurtt, G. C., Arneth, A., Brovkin, V., Calvin, K. V., Jones, A. D., et al. (2016). The Land Use Model Intercomparison Project (LUMIP) contribution to CMIP6: Rationale and experimental design. *Geoscientific Model Development*, *9*, 2973–2998. https://doi.org/10.5194/gmd-9-2973-2016

Lawrence, D., & Vandecar, K. (2014). Effects of tropical deforestation on climate and agriculture. *Nature Climate Change*, *5*, 27–36. https://doi.org/10.1038/nclimate2430

Le Quéré, C., Andrew, R. M., Friedlingstein, P., Sitch, S., Pongratz, J., Manning, A. C., et al. (2018). Global carbon budget 2017. *Earth System Science Data*, *10*(1), 405–448. https://doi.org/10.5194/essd-10-405-2018

Lejeune, Q., Davin, E. L., Gudmundsson, L., Winckler, J., & Seneviratne, S. I. (2018). Historical deforestation increased the risk of heat extremes in northern mid-latitudes. *Nature Climate Change*, *8*, 386–390. https://doi.org/10.1038/s41558-018-0131-z

Lejeune, Q., Seneviratne, S. I., & Davin, E. L. (2017). Historical land-cover change impacts on climate: Comparative assessment of LUCID and CMIP5 multimodel experiments. *Journal of Climate*, *30*, 1439–1459. https://doi.org/10.1175/JCLI-D-16-0213.1

Li, Y., Zhao, M., Mildrexler, D. J., Motesharrei, S., Mu, Q., Kalnay, E., et al. (2016). Potential and actual impacts of deforestation and afforestation on land surface temperature. *Journal of Geophysical Research: Atmospheres*, *121*, 14,372–14,386. https://doi.org/10.1002/2016JD024969

Li, Y., Zhao, M., Motesharrei, S., Mu, Q., Kalnay, E., & Li, S. (2015). Local cooling and warming effects of forests based on satellite observations. *Nature Communications*, *6*, 1–8. https://doi.org/10.1038/ncomms7603

Lorenz, R., Pitman, A. J., & Sisson, S. a. (2016). Does Amazonian deforestation cause global effects; can we be sure? *Journal of Geophysical Research: Atmospheres*, *121*, 5567–5584. https://doi.org/10.1002/2015JD024357

Mahmood, R., Roger A., Pielke, S., Hubbard, K. G., Niyogi, D., Dirmeyer, P. A., et al. (2014). Review—Land cover changes and their biogeophysical effects on climate. *International J of Climatology*, *34*, 929–953. https://doi.org/10.1002/joc.3736

Malyshev, S., Shevliakova, E., Stouffer, R. J., & Pacala, S. W. (2015). Contrasting local versus regional effects of land-use-change-induced heterogeneity on historical climate: Analysis with the GFDL Earth system model. *Journal of Climate*, *28*, 5448–5469. https://doi.org/10.1175/JCLI-D-14-00586.1

Meier, R., Davin, E. L., Lejeune, Q., Hauser, M., Li, Y., Martens, B., et al. (2018). Evaluating and improving the Community Land Model's sensitivity to land cover. *Biogeosciences*, *15*, 4731–4757.

Moss, R., Edmonds, J. A., Hibbard, K. A., Manning, M. R., Rose, S. K., van Vuuren, D., et al. (2010). The next generation of scenarios for climate change research and assessment. *Nature*, *463*, 747–756. https://doi.org/10.1038/nature08823

Pitman, A. J., de Noblet-Ducoudré, N., Cruz, F. T., Davin, E. L., Bonan, G. B., Brovkin, V., et al. (2009). Uncertainties in climate responses to past land cover change: First results from the LUCID intercomparison study. *Geophysical Research Letters*, *36*, L14814. https://doi.org/10.1029/2009GL039076

Pongratz, J., Raddatz, T., Reick, C., Esch, M., & Claussen, M. (2009). Radiative forcing from anthropogenic land cover change since A.D. 800. *Geophysical Research Letters*, *36*, L02709. https://doi.org/10.1029/2008GL036394

Pongratz, J., Reick, C. H., Raddatz, T., & Claussen, M. (2008). A reconstruction of global agricultural areas and land cover for the last millennium. *Global Biogeochemical Cycles*, *22*, GB3018. https://doi.org/10.1029/2007GB003153

Pongratz, J., Reick, C. H., Raddatz, T., & Claussen, M. (2010). Biogeophysical versus biogeochemical climate response to historical anthropogenic land cover change. *Geophysical Research Letters*, *37*, L08702. https://doi.org/10.1029/2010GL043010

Ramankutty, N., & Foley, J. A. (1999). Estimating historical changes in global land cover: Croplands from 1700 to 1992. *Global Biogeochemical Cycles*, *13*(4), 997–1027.

Reick, C. H., Raddatz, T., Brovkin, V., & Gayler, V. (2013). Representation of natural and anthropogenic land cover change in MPI-ESM. *Journal of Advances in Modeling Earth Systems*, *5*, 459–482. https://doi.org/10.1002/jame.20022

Rotenberg, E., & Yakir, D. (2010). Contribution of semi-arid forests to the climate system. *Science*, *327*, 451–454. https://doi.org/10.1126/science.1179998

Schultz, N. M., Lee, X., Lawrence, P. J., Lawrence, D. M., & Zhao, L. (2016). Assessing the use of subgrid land model output to study impacts of land cover change. *Journal of Geophysical Research: Atmospheres*, *121*, 6133–6147. https://doi.org/10.1002/2016JD025094

Stevens, B., Giorgetta, M., Esch, M., Mauritsen, T., Crueger, T., Rast, S., et al. (2013). Atmospheric component of the MPI-M earth system model: ECHAM6. *Journal of Advances in Modeling Earth Systems*, *5*, 146–172. https://doi.org/10.1002/jame.20015

Swann, A. L. S., Fung, I. Y., & Chiang, J. C. H. (2012). Mid-latitude afforestation shifts general circulation and tropical precipitation. *Proceedings of the National Academy of Sciences*, *109*, 712–716. https://doi.org/10.1073/pnas.1116706108

Winckler, J., Reick, C. H., Luyssaert, S., Cescatti, A., Stoy, P. C., Lejeune, Q., et al. (2018). Different response of surface temperature and air temperature to deforestation in climate models. *Earth System Dynamics Discussions*, 1–17. https://doi.org/10.5194/esd-2018-66

Winckler, J., Reick, C. H., & Pongratz, J. (2017a). Robust identification of local biogeophysical effects of land-cover change in a global climate model. *Journal of Climate*, *30*(3), 1159–1176. https://doi.org/10.1175/JCLI-D-16-0067.1

Winckler, J., Reick, C. H., & Pongratz, J. (2017b). Why does the locally induced temperature response to land cover change differ across scenarios? *Geophysical Research Letters*, *44*, 3833–3840. https://doi.org/10.1002/2017GL072519

Zhang, M., Lee, X., Yu, G., Han, S., Wang, H., Yan, J., et al. (2014). Response of surface air temperature to small-scale land clearing across latitudes. *Environmental Research Letters*, *9*(034002), 7. https://doi.org/10.1088/1748-9326/9/3/034002

Zwiers, F. W., & von Storch, H. (1995). Taking serial correlation into account in tests of the mean. *Journal of Climate*, *8*(2), 336–351. https://doi.org/10.1175/1520-0442(1995)008<0336:TSCIAI>2.0.CO;2